Moisture Absorption in Ionic Liquid Films

ARTICLE *in* THE JOURNAL OF PHYSICAL CHEMISTRY C · APRIL 2013

Impact Factor: 4.77 · DOI: 10.1021/jp400472d

THE JOURNAL OF PHYSICAL CHEMISTRY C

Article

pubs.acs.org/JPCC

Moisture Absorption in Ionic Liquid Films

José Restolho,[†,‡] José L. Mata,[†,§] Rogério Colaço,[†] and Benilde Saramago*[,†]

[†]Centro de Química Estrutural, Instituto Superior Técnico, Universidade Técnica de Lisboa, Avenida Rovisco Pais, 1049-001 Lisboa, Portugal

[‡]Research Institute for Medicines and Pharmaceutical Sciences, Faculty of Pharmacy, University of Lisbon, Avenida Prof. Gama Pinto, 1649-019 Lisboa, Portugal

[§]Academia Militar, Paço da Rainha, 29, 1150-244 Lisboa, Portugal

ABSTRACT: The uptake of water vapor by ionic liquids (ILs) has been studied by various research groups, but there is little knowledge on how liquid confinement affects the process of moisture absorption. In this work, several imidazolium-based ILs deposited on quartz crystals were used as water vapor sensors in a high sensitivity quartz-crystal microbalance with dissipation. The process of water vapor absorption by the IL films was interpreted, taking into account the changes of the different harmonics of the fundamental frequency. For the most viscous ILs, such as [C_2OHmim][BF_4] and [C_6mim]-[OAc], the decrease in viscosity was the dominant effect, while for the others, [C_8mim][BF_4], [C_2mim][OAc], and [C_4mim]-[OAc], the mass loading effect predominated. However, there are differences within the latter set: a gradual water adsorption and diffusion was observed in [C_2mim][OAc] and [C_4mim][OAc] films; in contrast, a discontinuity seems to have occurred between the formation of a water film on top of the [C_8mim][BF_4] film and its diffusion into the bulk. The kinetics of water absorption in the films of [C_2mim][OAc] and [C_4mim][OAc] was well described by a two-step model, and water diffusion coefficients in those films were obtained.

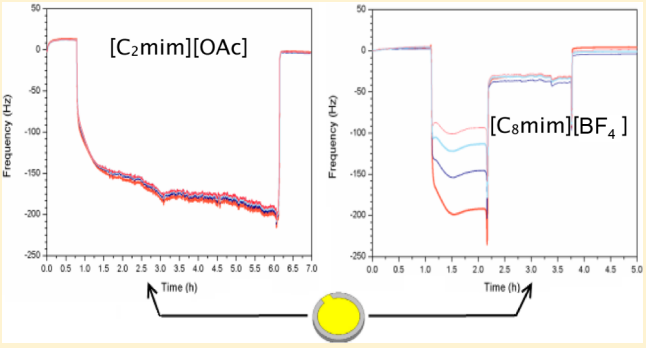

1. INTRODUCTION

For many years, piezoelectric devices have been used as sensors for organic vapors.[1] Detection was based on the measurement of the frequency shifts observed when the vapor adsorbed/absorbed onto the films deposited on the surface of gold-coated quartz crystals. The recent development of high sensitivity quartz-crystal microbalances with dissipation (QCM-D) led to renewed interest in that vapor detection technique.

Ceramics, polymers, self-assembled monolayers, and organic oils were the most commonly used materials to coat the gold surface of the quartz crystals.[1−4] In principle, liquids would be attractive sensing materials because they are in thermodynamic equilibrium and they enable fast diffusion of the analytes. Ionic liquids (ILs) have the exact characteristics to be considered as excellent gas sensors. They are liquids with vanishing vapor pressures at ambient temperature, which solves the problem of liquid evaporation. On the other hand, a broad range of functionalities in the side groups of the ionic liquids may be chosen in order to ensure the wettability of the sensor surface and/or the affinity toward the specific organic vapor.

The usage of ionic liquids as sensing materials for QCM-based vapor-sensing devices was first reported in 2002 by Liang et al.[5] They demonstrated that the responses of the ionic liquid based QCM device toward a vapor depended on the types of cations and anions present, and they interpreted the frequency shifts as the result from the plasticization of the ionic liquids induced by the vapor sorption. In addition, they claimed that the mass transport rates of analytes in ionic liquids were much faster than those observed for solid inorganic or organic coatings. Goubaidoulline et al.[6] used a sensor where the ionic liquid was contained in the pores of a nanoporous alumina layer, formed on the front electrode of the quartz crystal by anodization. This concept is the basis of the supported ionic liquid phase (SILP) materials which have the advantage of increasing the rate of mass transfer through the extension of the surface area of the exposed ionic liquid. Shen et al.[7] studied the adsorption process of acetone vapor into a film of 1-octyl-3-methylimidazolium bromide ([C_8mim][Br]) deposited on Y-cut langasite crystal resonators. Recently, ionic liquid films deposited on quartz crystal sensors have been used in the detection of volatile organic compounds (VOCs).[8,9]

Most of the above-referred studies focused mainly the uptake of vapors and the affinity of various ILs for specific analytes, but a deep understanding of the behavior of IL films when the analyte molecules interact with them is still missing. In particular, knowledge of the interaction of water vapor with IL films is of special importance because (1) the presence of water may be responsible for the special affinity of the IL toward specific analytes and (2) water vapor has a known interference to IL based QCM sensors.[10] To contribute to the

Received: January 15, 2013
Revised: April 3, 2013
Published: April 23, 2013

Table 1. Structure, Solubility in Water, and Cation Hydrophobicity Parameter (log $k_{0,c}$) of the Studied Ionic Liquids

IL	Structure	Water Solubility % w/w	Cation hydrophobicity parameter
[C_2mim][OAc]	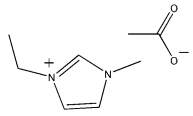	-	0.22[c]
[C_4mim][OAc]	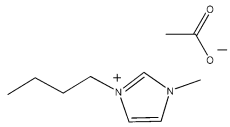	-	0.67[c]
[C_6mim][OAc]	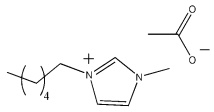	-	1.2[c]
[C_2OHmim][BF_4]	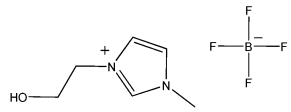	∞[a]	-0.28[d]
[C_8mim][BF_4]	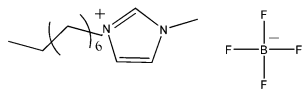	10.3[b]	1.9[c]

[a]Taken from ref 14. [b]Taken from ref 15. [c]Taken from ref 11. [d]Taken from ref 16.

elucidation of the mechanism of water vapor interaction with ionic liquid films was the aim of this work. Films of a series of ionic liquids deposited by spin-coating on the gold surface of quartz crystals were exposed to the flow of saturated water vapor, and the resulting changes in their viscoelastic properties were assessed using a QCM-D. The structure of the ionic liquid films was investigated by imaging with an atomic force microscope (AFM). From the time dependence of the QCM-D data, the kinetics of the water absorption process was determined.

Two series of ionic liquids were studied: one based on the acetate anion, 1-ethyl-3-methylimidazolium acetate, [C_2mim][OAc], 1-butyl-3-methylimidazolium acetate, [C_4mim][OAc], and 1-hexyl-3-methylimidazolium acetate, [C_6mim][OAc]; and the other based on the tetrafluoroborate anion, 1-ethanol-3-methylimidazolium tetrafluoroborate, [C_2OHmim][BF_4], and 1-octyl-3-methylimidazolium tetrafluoroborate, [C_8mim][BF_4]. In the former case the effect of the length of the alkyl R substituent on the imidazolium cation [Rmim] was addressed in a family of ionic liquids based on a halogen-free anion, while in the latter two well-characterized ionic liquids with quite different polarities were investigated. The structures, solubilities in water, and values of the cation hydrophobicity parameter (defined as log $k_{0,c}$ according to ref 11) of the studied ionic liquids are presented in Table 1. As expected,[12] the hydrophobicity of the cation increases in the series ethyl, butyl, hexyl, octyl, while [C_2OHmim] is the most hydrophilic. Although no values of the solubility in water for the [Rmin][OAc] could be found in the literature, these ionic liquids are known to form strong hydrogen bonds with water,[13] which should imply a very high solubility. This means that, among the ILs investigated, only [C_8mim][BF_4] has a limited solubility in water.

2. EXPERIMENTAL SECTION

2.1. Materials. The ionic liquids 1-alkyl-3-methylimidazolium acetate, [$C_n$mim][OAc], with n = 2, 4, and 6; 1-ethanol-3-methylimidazolium tetrafluoroborate, [C_2OHmim][BF_4]; and 1-octyl-3-methylimidazolium tetrafluoroborate, [C_8mim][BF_4], were purchased from Solchemar (Portugal) with purities of >98%. The purities of the ionic liquids were checked by NMR after the synthesis. The water content, checked by Karl Fischer titration, was ≈600 ppm for [C_2mim][OAc], 300 ppm for [C_4mim][OAc], 400 ppm for [C_6mim][OAc], 344 ppm for [C_8mim][BF_4], and 800 ppm for [C_2OHmim][BF_4]. The chlorine content, determined with a selective Cl-electrode, was <50 ppm. Toluene and acetone were from Panreac, ethanol was from AGA, and (3-aminopropyl)triethoxysilane was from Fluka. Milli-Q water was used in all experiments.

The AT-cut 5 MHz piezoelectric quartz crystals (14 mm diameter) coated with gold were supplied by Q-Sense (Gothenburg, Sweden). For the contact angle measurements, substrates of poly(tetrafluoroethylene) (PTFE) sheet with 1 mm thickness (Goodfellow) were used.

2.2. Methods. The contact angle measurements were carried out by the sessile drop method using the ADSA-P software (Axisymetric Drop Shape Analysis, Applied Surface Thermodynamics Research Associates, Toronto, Canada) for image analysis. During the experiments, the chamber was flushed with pure, dry nitrogen. Further experimental details may be found in ref 17. The contact angles were measured at

dx.doi.org/10.1021/jp400472d | J. Phys. Chem. C 2013, 117, 10454−10463

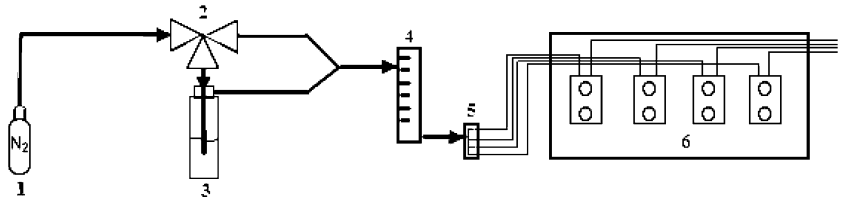

Figure 1. Experimental setup for the QCM-D gas sensing experiments: 1, nitrogen cylinder; 2, three-way valve; 3, water container; 4, flowmeter; 5, tubing distributor; 6, Q-Sense stage.

room temperature. The contact angle evolution over time was recorded, for time intervals ranging from 10 to 60 min, depending on the liquid spreading kinetics. When a plateau was achieved, the so-called static contact angle was recorded. The density values, which are necessary for the experimental determination of the surface tension, were measured with an Anton-Paar DMA 5000 vibrating-tube densimeter in the temperature range 298−363 K. All reported density data were corrected for the effect of viscosity using the internal calibration of the densimeter. To prevent the effect of air bubbles, each measurement was repeated twice. The viscosity was measured with an automated SVM 3000 Anton Paar rotational Stabinger viscometer−densimeter. The temperature uncertainty was ±0.02 K, while the precision of the dynamic viscosity measurements was ±0.5%. The overall uncertainty of the measurements was reported to be 2%.[18]

A Q-Sense quartz crystal microbalance with dissipation (Model E4) was used to assess the adsorption/absorption of the water vapor on the IL films. The experiments were done at 25 °C and the results are averages of, at least, four independent measurements. Prior to the measurements, all the QCM-D balance parts were sonicated 5 min in a 10% alkaline cleaning solution of Extran and then twice in Milli-Q water, followed by blow drying with nitrogen. The quartz crystals were carefully cleaned according to the same protocol and finally dried during 2 h inside a vacuum oven at room temperature. After drying, the crystals were submitted to two successive 10 min UV/ozone treatments, separated by rinsing with Milli-Q water. To achieve complete spreading of the ionic liquids, polar surfaces were prepared with a silane containing amino groups, according to the procedure described by Batchelor et al.[19] The crystals were then submersed in 10 mL of 5% (w/w) toluene solution of (3-aminopropyl)triethoxysilane and stored at room temperature overnight. After completion of the reactions, the crystals were isolated and rinsed sequentially with toluene, acetone, and water, blown with nitrogen, and dried during 2 h inside a vacuum oven. The only sample which did not wet the silanized gold surface was $[C_2OHmim][BF_4]$. The amine-terminated surface was further used to prepare a surface with trimethylammonium groups, but complete spreading was not achieved. In this case, the best solution was to use the UV/ozone treated gold substrate where the contact angle of $[C_2OHmim][BF_4]$ was 53°, still much higher than the contact angles of the other ILs on silanized gold (e.g., 19° for $[C_8mim][BF_4]$).

The wetting films of ILs were deposited by spin-coating, at 2000 rpm during 40 s, from ethanol (99.5% purity grade) solutions with a concentration of 2.5 mg·mL^{-1} on freshly prepared silanized quartz crystals. After deposition, the samples were kept under vacuum until imaging. The IL films were studied at 24 h after film production due to the known time dependence of the film structure.[20]

Figure 1 shows a scheme of the experimental arrangement for water vapor adsorption on the IL film. A saturated water vapor stream was obtained by passing dry nitrogen through a liquid water reservoir. The inlet QCM tubes are connected via a three-way valve to allow admission of dry nitrogen or water-saturated nitrogen. A typical QCM-D experiment consists of the following steps: (1) injection of a constant dry nitrogen flow (850 mm^3·s^{-1} measured with an Omega FL5511g flowmeter) into the measuring cells, (2) replacement of dry nitrogen by the same flow of nitrogen saturated with water vapor, and (3) final rinsing with dry nitrogen. Each step is performed until stabilization of the frequency shift is achieved. The normalized frequency shift, Δf (change in frequency divided by the harmonic number), and the dissipation, ΔD, are recorded for the n harmonics of the fundamental frequency (n = 3, 5, 7, 9, and 11) against time.

A Veeco DI CPII atomic force microscope (AFM) was used for the visualization of the ionic films. The AFM was operated in contact mode using Si tips with a spring constant of 0.9 N·m^{-1} at a constant contact force of 100 nN. These conditions were the only ones that enable obtaining AFM images with an acceptable level of noise in all of the observed samples. To guarantee that visualization in contact mode does not interfere with the film topography, successive scans at increasing lengths were made. Topographic images were recorded only if no changes in the successive scans were detected, either in topography or in lateral force mode.

3. RESULTS AND DISCUSSION

3.1. Ionic Liquid Characterization. The densities of the ionic liquids vary linearly with the temperature according to the following equations: ρ/g·cm^{-3} = 1.5260 − 7.0 × 10^{-4}T/K for $[C_2mim][OAc]$, ρ/g·cm^{-3} = 1.2504 − 6.0 × 10^{-4}T/K for $[C_4mim][OAc]$, and ρ/g·cm^{-3} = 1.3621 − 7.0 × 10^{-4}T/K for $[C_6mim][OAc]$, with uncertainties of ±0.00016, ±0.00018, and ±0.00027 g·cm^{-3}, respectively. The densities of $[C_8mim][BF_4]$ and $[C_2OHmim][BF_4]$, respectively equal to ρ/g·cm^{-3} = 1.3244 − 6.0 × 10^{-4}T/K and ρ/g·cm^{-3} = 1.1171 − 7.0 × 10^{-4}T/K, were taken from a previous work.[21]

The surface tensions and the viscosities at ambient temperature (298 K) of the ILs are shown in Table 2: for those based on the anion acetate the values were taken from refs 13 and 22, while those for the other two liquids were previously measured in our laboratory.[21] The contact angles on PTFE, averaged over at least four measurements, are also presented in Table 2.

The polarities of the ILs were estimated from the surface tensions and the contact angles using the approach of Fowkes.[23] According to this approach, the surface tension, γ_L, of a solid or a liquid can be described as a sum of independent contributions each arising from the intermolecular interactions present in such phases. For practical reasons it is common to

Table 2. Surface Tension, Contact Angle on PTFE, Polarity Fraction (γ_L^{nd}/γ_L), and Viscosity of the Ionic Liquids, at 298 K[a]

IL	surf. tension ($mJ \cdot m^{-2}$)	contact angle (deg)	polarity fraction	viscosity (Pa·s)
$[C_2mim][OAc]$	41.0[b] (127 ppm)	77.5	0.39	0.162[c] (120 ppm)
$[C_4mim][OAc]$	39.4[b] (147 ppm)	70.2	0.30	0.485[c] (85 ppm)
$[C_6mim][OAc]$	36.1[b] (128 ppm)	61.9	0.22	1.710 (400 ppm)
$[C_2OHmim][BF_4]$	64.9[d] (800 ppm)	100.6[e]	0.38[e]	0.97[d] (800 ppm)
$[C_8mim][BF_4]$	32.9[d] (344 ppm)	80.4[e]	0.32[e]	0.32[d] (344 ppm)

[a]The water contents of the ILs are given in parentheses. [b]Taken from ref 13. [c]Taken from ref 22. [d]Taken from ref 21. [e]Taken from ref 17.

include all the nondispersive interactions in a single term so that

$$\gamma = \gamma_i^d + \gamma_i^{nd} \quad (1)$$

where subscript i = S or L indicates, respectively, the solid or the liquid, while superscripts "d" and "nd" stand for the dispersive and nondispersive terms of the surface tension. Assuming that the dispersive forces between pairs of unlike molecules may be described by the geometric mean rule, the following relation was deduced:[24]

$$\gamma_L(1 + \cos\theta) = 2(\gamma_S^d \gamma_L^d)^{1/2} \quad (2)$$

The dispersive component of the surface tension of a liquid may then be calculated from its contact angle, θ, on a purely dispersive solid, once γ_L and $\gamma_S^d = \gamma_S$ are known. The nondispersive component is obtained using eq 1. This assumption is valid when both phases are nonpolar and may be a good estimate when only one of them is polar. The polarity fraction is then defined as the ratio between the nondispersive component, γ_L^{nd} (often called the "polar" component), and the total surface tension. Assuming that PTFE is a purely dispersive solid with a surface tension of 17.5 $mJ \cdot m^{-2}$,[25] the polarity fractions were calculated and are given in Table 2.

All ionic liquids may be classified as moderately polar, with the exception of $[C_6mim][OAc]$, whose polarity is lower than the typical values of imidazolium-based ionic liquids.[17] Within the acetate-based family, polarity decreases with increasing cation hydrophobicity parameter (see Table 1) which correlates directly with the length of the alkyl R substituent in the cation. Viscosity is strongly dependent on the anion. For the acetate-based series, viscosity increases with the alkyl chain length, but a long chain length of the cation C_8mim associated with the BF_4 anion dictates a relatively low viscosity.

3.2. AFM Imaging. Figure 2a–d shows AFM images of the IL films obtained after 24 h of film deposition. Images of the film obtained with $[C_2OHmim][BF_4]$ could not be acquired, because in contact conditions its adhesion to the substrate was so low that the tip became readily contaminated and dragging of the liquid occurred, and in noncontact conditions the sticky behavior of the film introduces unacceptable noise in the AFM images. The surface of bare silanized gold (Figure 2e) has the typical granular topography where the roundish features have average height of the order of 4–5 nm and an x-periodicity of the order of 50 nm. In the images of the IL films, this topography is no longer seen in between the droplets, as shown in the smaller length topographic profiles of Figure 2a–d. This result indicates that the thickness of the deposited films is enough to hide the underlying structure. All films exhibit the drop-on-the-layer behavior characteristic of IL films deposited from concentrated solutions (IL concentration ≥ 0.5 $mg \cdot mL^{-1}$) on hydrophilic substrates. Similar images were reported in a recent work involving films of $[C_8mim][BF_4]$ deposited on a solid aluminum where liquidlike lamellar structures were observed.[20]

However, it is possible to identify clear differences among the films obtained with the various ILs. The $[C_8mim][BF_4]$ film (Figure 2d) stands out due to the very high number of liquid drops of small and uniform dimensions. The small drop coalescence observed may be explained by the low values of the surface tension and the viscosity of this IL (see Table 2). Since these properties are related to the strength of the interactions that are established between the cations and the anions, the mean cohesive energy both at the surface and in the bulk of $[C_8mim][BF_4]$ should be minimum in comparison with those of the other studied ILs.

In contrast, the films obtained with the acetate-based ILs exhibit a smaller number of drops and a large distribution of drop sizes. The drops of larger height (120 nm) are found in $[C_2mim][OAc]$ (Figure 2a). It is interesting to notice that, within the series of the acetate-based IL films, those of $[C_6mim][OAc]$ presented the lowest adhesion to the substrate which resulted in some dewetting that can be detected in the inferior left corner of the image (Figure 2c). This behavior in the presence of a highly hydrophilic substrate may be attributed to the low polarity fraction of this liquid (see Table 2). In the case of $[C_2OHmim][BF_4]$, the very small affinity to the hydrophilic substrate (average contact angle of 53°) is not consistent with its high polarity fraction, but should rather be ascribed to strong hydrogen forces between anion and cation that hinder their preferential interaction with the solid substrate.

3.3. QCM-D Experiments. Figure 3 represents typical results of QCM-D experiments obtained with films of the five ILs tested. Taking the first addition of dry nitrogen as the baseline, the subsequent changes correspond to the interaction of the IL film deposited on the surface of the crystal with the nitrogen saturated with water vapor, followed by rinsing with the dry nitrogen.

Interpretation of QCM-D data when the resonance frequency decreases due to an increase in mass (adsorption) may be based on the Sauerbrey equation,[26] if the adsorbed film is rigid, or on the modified Sauerbrey equation if the film is viscoelastic.[27] When the change in resonance frequency is associated with the variation of the medium viscosity/density, then the equation of Kanazawa and Gordon[28] should be applied. However, in several applications the QCM-D sensor is simultaneously loaded by a rigid surface mass layer and a contacting Newtonian liquid. Martin et al.[29] solved a continuum electromechanical model to calculate the change in resonant frequency obtained in these circumstances. When mass and liquid loading are small, the normalized change in frequency, Δf, is given by

dx.doi.org/10.1021/jp400472d | J. Phys. Chem. C 2013, 117, 10454–10463

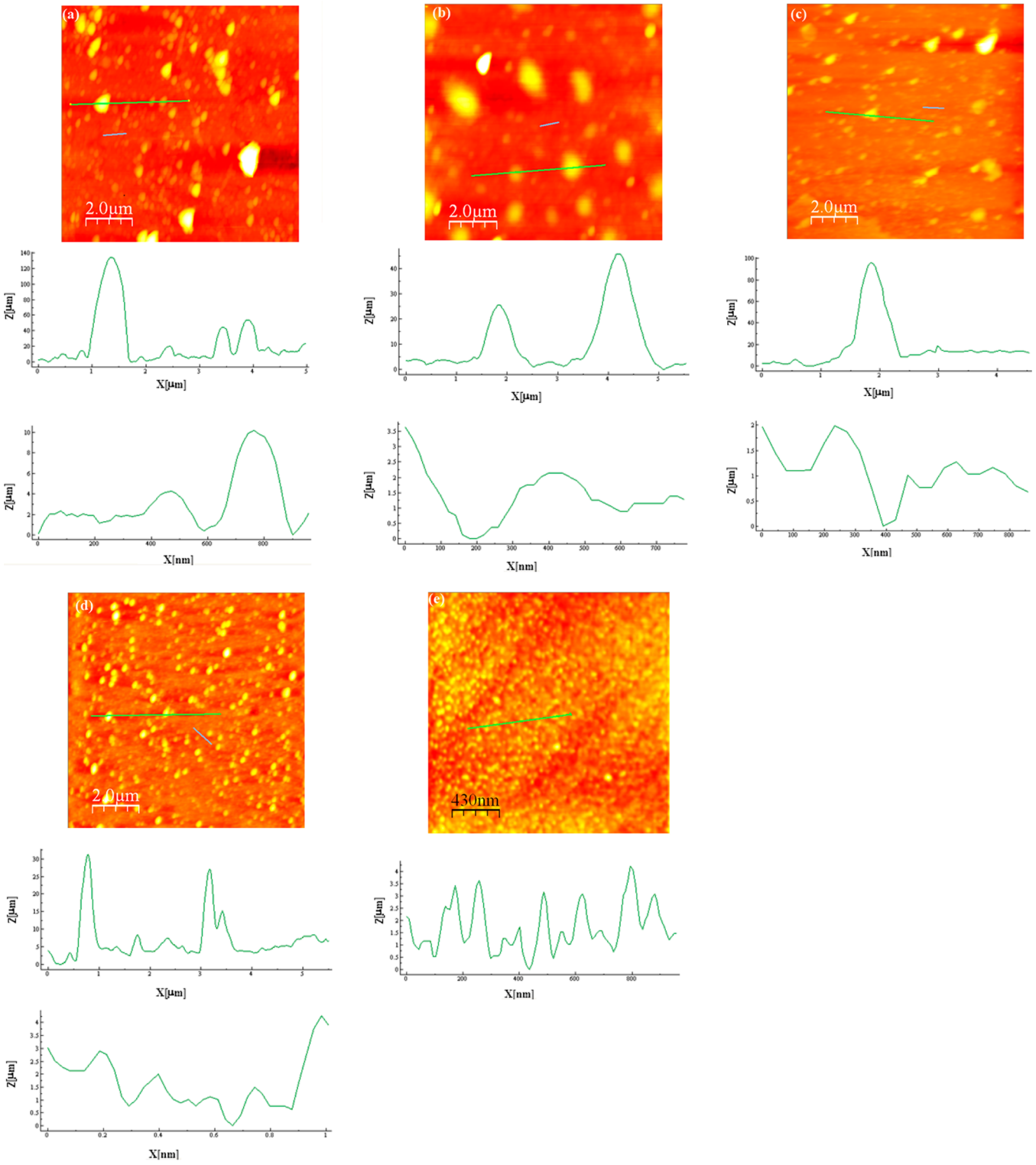

Figure 2. AFM topographic images of films obtained with (a) [C_2mim][OAc], (b) [C_4mim][OAc], (c) [C_6mim][OAc], and (d) [C_8mim][BF_4] on a silanized gold surface recorded at 24 h after film deposition. The image of the bare silanized gold surface (e) is included for comparison purposes. Height profiles are shown below each image.

$$\Delta f = -\frac{2f_0^{\,2}}{(\mu_Q \rho_Q)^{1/2}}\left[\rho_f h_f + \left(\frac{\rho_L \eta_L}{4\pi f_0}\right)^{1/2}\right] \quad (3)$$

where f_0 is the fundamental frequency of the crystal; μ_Q and ρ_Q are, respectively, the elastic modulus and the density of the quartz; ρ_f and h_f are, respectively, the density and the thickness of the surface layer; $\rho_L$and η_L are, respectively, the density and the viscosity of the liquid. When the mass loading is dominant, eq 3 reduces to the first term, which is equivalent to the Sauerbrey equation; in contrast, when the mass loading is negligible in comparison with the liquid loading, eq 3 reduces

dx.doi.org/10.1021/jp400472d | J. Phys. Chem. C 2013, 117, 10454−10463

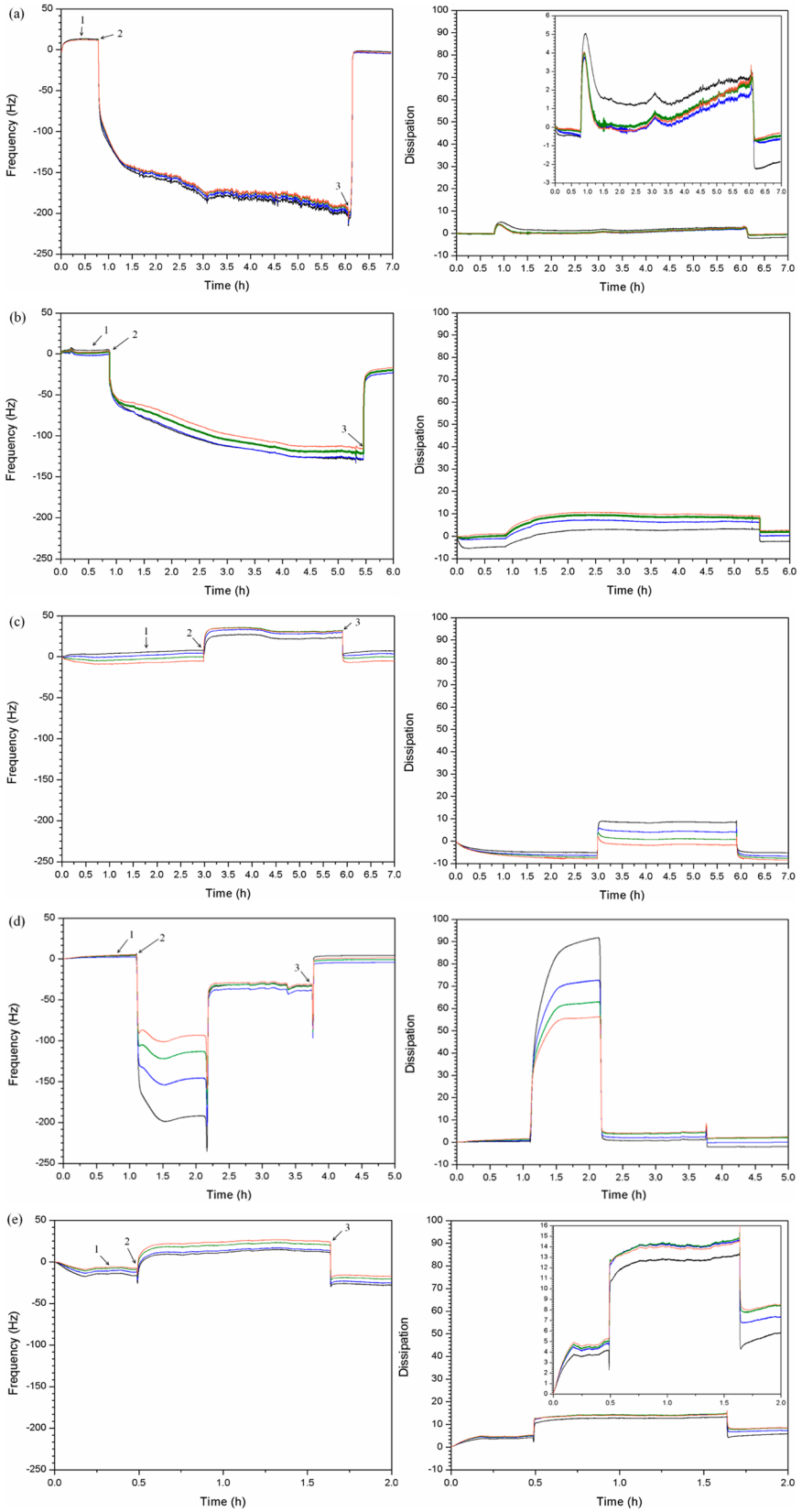

Figure 3. Variation of the (left) normalized frequency $\Delta f/n$ and (right) dissipation ΔD for all harmonics of the fundamental frequency (n = 3, black; n = 5, blue; n = 7, green; n = 9, orange) in a typical experiment consisting of (1) contact of the IL film with dry nitrogen, (2) addition of water vapor, and (3) rinsing with dry nitrogen. The ILs are (a) [C_2mim][OAc], (b) [C_4mim][OAc], (c) [C_6mim][OAc], (d) [C_8mim][BF_4], and (e) [C_2OHmim][BF_4]. Insets with expanded views are added whenever the curves are indistinguishable.

dx.doi.org/10.1021/jp400472d | J. Phys. Chem. C 2013, 117, 10454−10463

to the second term, which is equivalent to the Kanazawa and Gordon equation.

For the most viscous ionic liquids, [C_6mim][OAc] and [C_2OHmim][BF_4] (Figure 3c,e), the interaction with water vapor led to an increase in both frequency and dissipation which may be attributed to a reduction of the damping effect associated with the decrease in the IL viscosity, η_L. By contrast, the less viscous liquids, [C_2mim][OAc] and [C_4mim][OAc] (Figure 3a,b), suffered a decrease in frequency (respectively, $\Delta f \sim -200$ Hz and $\Delta f \sim -130$ Hz for the third harmonic) and an increase in dissipation which are consistent with the increase in mass, $\rho_f h_f$, due to water adsorption. The behavior of [C_8mim][BF_4] (Figure 3d) is different from that observed with the pairs of ILs just referred. The frequency decreased continuously with time achieving a constant value and, after approximately 1 h, increased spontaneously leading to a final constant value of $\Delta f \sim -50$ Hz. Furthermore, the decrease in frequency is accompanied by a huge increase in dissipation which is characteristic of a fluidic material and, then, spontaneously decreases to very low values as the frequency increases. This strange behavior could be attributed to a two-step process where the first stage is dominated by the increase in mass followed by a decrease in density and/or viscosity. Comparison of the equilibrium frequency shifts obtained with these three ILs shows an increase in the water uptake according to the decreasing value of hydrophobicity parameter of the cations (see Table 1).

A deeper analysis of the QCM-D results, taking into consideration the variation of the different harmonics of the fundamental frequency, may help in the interpretation of the results. It is known that the higher order harmonics are more sensitive to the modifications at the solid interface while those of lower order "feel" the liquid interface of the supported IL. The QCM-D results show that, for [C_2mim][OAc] and [C_4mim][OAc], all harmonics have similar negative frequency shifts and similar increases in dissipation, which is consistent with the presence of a relatively rigid IL film. In contrast, for [C_8mim][BF_4] the lower order harmonics are the most affected in a first step, suggesting that the changes of the IL film occurred mostly at the upper interface, followed by a second step where the frequency increases, dissipation decreases, and all harmonics practically coincide. This may indicate a gradual water adsorption and diffusion through the films of [C_2mim][OAc] and [C_4mim][OAc], while in the films of [C_8mim][BF_4] a discontinuity occurs between the formation of a metastable water film on top of the IL which then disappears by evaporation and/or diffusion through the IL.

Further analysis of Figure 3 shows that, after rinsing with the dry nitrogen, the frequency and dissipation of all ionic liquid films rapidly recover the initial values, in the case of both positive and negative frequency shifts. This means that the internal rearrangement in the IL film structure associated with the process of dissolution and removal of the water molecules is practically reversible.

3.4. Data Correlation. In a recent publication[30] describing water absorption by anhydrous ionic liquids, the interpretation of the interaction of water vapor with IL films was done in terms of three phenomena: (1) the adsorption of water molecules on the IL surface, (2) their diffusion into the IL, and (3) the formation of water−ion complexes when the IL samples have a non-negligible thickness. According to the same authors, each phenomenon depended on different IL features. Water adsorption depends on the affinity of water for the groups exposed on the IL free surface, while diffusion is largely affected by the liquid viscosity which strongly depends on water concentration. Other authors considered the water uptake of ILs in contact with the atmospheric humidity as the result of adsorption and the formation of a water film on the IL surface.[31]

In general, both hydrophilic and hydrophobic ILs absorb water at a high speed, but hydrophilic ILs absorb a higher amount. It is known that anions usually determine water absorption, while water solubility depends mainly on the cation, decreasing when the length of the alkyl chain on the cation increases.[32] The interactions responsible for the solubility of water vapor in an ionic liquid are not only determined by hydrophobicity but also other factors, such as stereochemistry and polarity, play a role.

The presence of [OAc] and [BF_4], water binding anions, on the IL surface favors the water adsorption and, at the same time, should reduce the rate of water diffusion inside the IL. Furthermore, it was recently demonstrated that water diffusivity inside [C_2mim][OAc] depends on the water concentration.[31] The water self-diffusivity increases at high water concentrations, probably due to the decrease in the interactions between water and the IL.

Comparison of the behavior of the less viscous ionic liquid films, [C_2mim][OAc], [C_4mim][OAc], and [C_8mim][BF_4], suggests that water interacts with the surfaces of these films in different ways, in spite of the known water affinity to both anions. In a recent investigation on wetting films of ILs,[33] some of the authors concluded that the main forces which are responsible for the stability of thin films of [C_8mim][BF_4] are dispersive interactions between the long alkyl chains of the cations segregated at the surface. In this case, the water molecules have weak affinity to the hydrophobic interface and form a liquid deposit whose viscoelastic properties are revealed by the discrepancy among the various harmonics. Only after a certain period of time, during which the ions at the surface may undergo reorientation, water molecules are able to penetrate and diffuse into the IL film. However, the amount of water absorbed is low ($\Delta f \sim -50$ Hz) due to the limited water solubility of this IL. In contrast, it is expected that, for the acetate-based ILs, hydrogen bonds between water and acetate anions are responsible for a fast adsorption and absorption process that leads to an increase in mass.

In order to further understand the mechanism of water diffusion, the Fickian model, which is the easiest one for water absorption in a thin film, was applied. At short times, the relative mass increase can be written as

$$\frac{M_t}{M_\infty} = \frac{2}{h}\sqrt{\frac{Dt}{\pi}} \tag{4}$$

where M_t and M_∞ are, respectively, the mass gains at time t and at equilibrium, h is the film thickness, and D is the water diffusivity.[4] In [C_2mim][OAc] and [C_4mim][OAc] the films present a nonviscoelastic behavior because the dissipation is low and the frequency shifts correspondent to the various harmonics almost coincide. The mass of water absorbed on the IL film can thus be determined from the change in the resonance frequency using the Sauerbrey equation. Considering that the ratio of masses, M_t/M_∞, is equal to the ratio of frequency shifts, $\Delta f_t/\Delta f_\infty$, where Δf_t and Δf_∞ are, respectively, the frequency changes at time t and at equilibrium, it is possible to fit the linear part of the experimental data to eq 4, assuming a

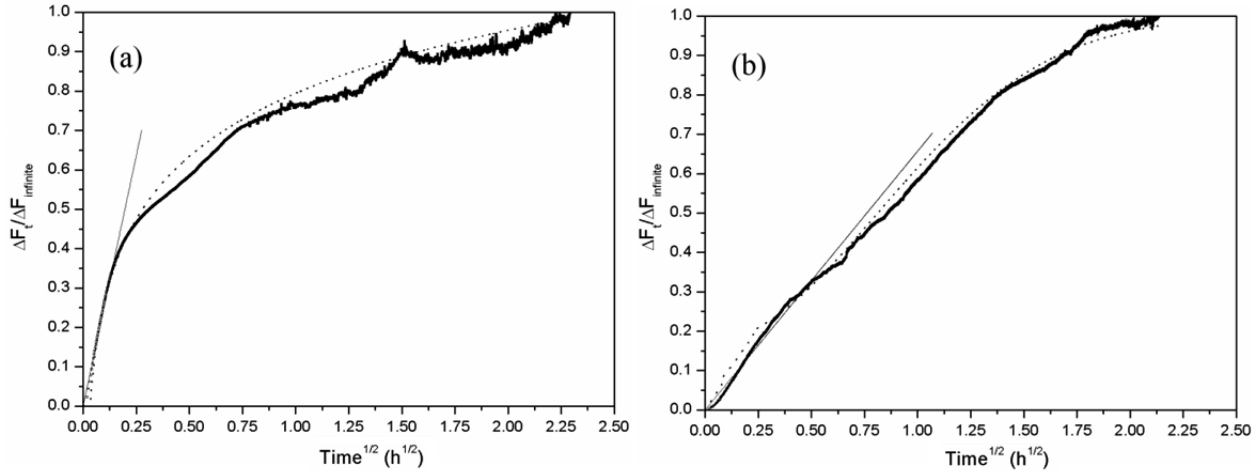

Figure 4. Relative mass increase of the (a) [C_2mim][OAc] and (b) [C_4mim][OAc] films due to water absorption (thick lines resulting from the superposition of a great number of experimental points). Data were fitted to the Fickian model (thin lines) and to variable-surface concentration two-step model (dashed lines).

Table 3. Fitting Parameters of Film Thickness, h, and Water Diffusion Coefficient, D, Obtained with eq 4 and Dimensionless Numbers ϕ and ψ Determined Using eq 5[a]

IL	h (nm)	D ($m^2 \cdot s^{-1}$)	R^2 (eq 4)	ϕ	ψ	R^2 (eq 5)
[C_2mim][OAc]	180	4.70×10^{-17}	0.9897	7.5×10^{-4}	0.09	0.9930
[C_4mim][OAc]	180	3.05×10^{-18}	0.9767	2.8×10^{-4}	2.39	0.9915

[a]The quadratic correlation coefficients, R^2, characterize the fittings to both equations.

reasonable value for the film thickness. Unfortunately, we were not able to get a meaningful value for the film thickness from ellipsometric measurements because an adequate model for this complex system could not be found. However, we may assume a value in the range 150−200 nm taking into consideration that the height of the highest drops on top of the underlying layer was 120 nm (AFM images in Figure 2). The experimental values of $\Delta f_t/\Delta f_\infty$ are plotted as a function of $t^{1/2}$ in Figure 4.

The mass of the film increases rapidly in the first minutes, followed by a slower pace that continues until equilibrium. The initial slope has a Fickian behavior which allows the calculation of the film thicknesses and of the diffusion coefficients of water in [C_2mim][OAc] and in [C_4mim][OAc]. The values of these parameters (respectively, h and D) resulting from the linear fittings are shown in Table 3. The second stage exhibits a non-Fickian behavior which is not diffusion controlled. Several theoretical models have been proposed to describe two-step absorption processes.[34] The variable surface concentration model proposed by Long and Richman has been successfully applied to fit experimental data. According to this model,[34] the absorption process results from two independent contributions: a diffusion controlled part (governed by Fick's law) and a relaxation controlled part. Assuming only a first-order relaxation process, the fractional mass uptake at time t can be described as the linear superposition of both contributions (eq 5):

$$\frac{M_t}{M_\infty} = \phi\left[1 - \frac{8}{\pi^2}\sum_{n=0}^{\infty}\frac{\exp\left(\frac{-(2n+1)^2\pi^2\theta}{4}\right)}{(2n+1)^2}\right] + (1-\phi)\left[1 - \frac{\tan\sqrt{\psi}\,e^{-\psi\theta}}{\sqrt{\psi}} - \frac{8}{\pi^2}\sum_{n=0}^{\infty}\frac{\exp\left(\frac{-(2n+1)^2\pi^2\theta}{4}\right)}{(2n+1)^2\left(1-\frac{(2n+1)^2\pi^2}{4\psi}\right)}\right] \quad (5)$$

where $\phi = C_0/C_\infty$, $\theta = Dt/h^2$, $\psi = kh^2/D$, and k is the rate constant of the relaxation process. The dimensionless number ϕ represents the ratio of the water concentration at the film surface immediately after contacting the vapor, C_0, to the final concentration, C_∞, and the dimensionless number ψ is the ratio between the characteristic diffusion time and the characteristic relaxation time.

It is important to remark that this model has the advantage of having only four parameters to fit, where two of them (h and D) can be obtained from the initial slope using eq 4. Starting with the values of h and D previously determined, the data were fitted to eq 5, and the resulting curves are shown in Figure 4 while parameters ϕ and ψ are given in Table 3. Small values of ψ mean that the relaxation time is larger than the diffusion time, which is the case in the [C_2mim][OAc] films but not in the [C_4mim][OAc] films. In both cases the values of ϕ are very small, meaning that the amount of relaxation controlled absorption is very large.

Although we could not find in the literature any values for the diffusion coefficient of water in ionic liquid films, we may

dx.doi.org/10.1021/jp400472d | J. Phys. Chem. C 2013, 117, 10454−10463

compare our results with the bulk diffusion coefficients of water in [C_2mim][OAc] recently reported by Shi et al.[32] These values varied between 5×10^{-11} and 1×10^{-10} $m^2 \cdot s^{-1}$ depending on the water mole fraction. The difference in the order of magnitude between this set of values and those presented in Table 3 may be explained by the effect of liquid confinement. Although this issue is controversial, several authors[4,35] claimed that water mobility in films decreases in relation to their bulk values. Namely, Vogt et al.[4] found a decrease in the diffusion coefficient of water in polyelectrolyte films from 3×10^{-17} to 5×10^{-21} $m^2 \cdot s^{-1}$ when the film thickness decreased from 200 to 2 nm. The lower value of the diffusion coefficient for [C_4mim][OAc] in comparison with that of [C_2mim][OAc] may be attributed to the longer length of the alkyl substituent of the former cation which is responsible for its higher hydrophobicity.

Finally, we should remark that the most viscous ionic liquids, [C_6mim][OAc] and [C_2OHmim][BF_4], formed films with low adhesion to the substrate surface. While good quality AFM images of the latter could not be obtained for this reason, the films of the former revealed noncoated areas on the gold surface. These heterogeneous films may experience a large damping effect which is characteristic of a viscoelastic medium.

4. CONCLUSIONS

Films of several imidazolium-based ILs were deposited on quartz crystals to be used as water vapor sensors. Two distinct behaviors were observed upon interaction with water vapor: for the films of the most viscous ILs, such as [C_2OHmim][BF_4] and [C_6mim][OAc], the decrease in viscosity was the dominant effect, while for the others, [C_8mim][BF_4], [C_2mim][OAc], and [C_4mim][OAc], the mass loading effect predominated.

Analysis of the changes of the different harmonics of the fundamental frequency obtained with the less viscous liquids seems to indicate a gradual water adsorption and diffusion through the films of [C_2mim][OAc] and [C_4mim][OAc], while for [C_8mim][BF_4] a discontinuity occurs between the formation of a water film on top of the IL which then diffuses into the bulk, leading to a decrease in the film viscosity.

Application of the Fickian model to water absorption at short times allowed the calculation of water diffusion coefficients in the films of [C_2mim][OAc] and [C_4mim][OAc]. These values are much smaller than the bulk values which may be attributed to the effect of liquid confinement. Further analysis of the kinetics of water absorption was done using the Long and Richman variable surface concentration model which considers two stages: diffusion controlled (governed by Fick's law) and relaxation controlled. According to this model, the relaxation time is larger than the diffusion time in the case of [C_2mim][OAc] and smaller for [C_4mim][OAc].

AUTHOR INFORMATION

Corresponding Author

*Tel.: 351 218419226. Fax: 351 218419239. E-mail: b.saramago@ist.utl.pt.

Notes

The authors declare no competing financial interest.

ACKNOWLEDGMENTS

We are indebted to Dr. José Esperança from ITQB for the viscosity measurements. J.R. acknowledges Fundação para a Ciência e Tecnologia (FCT) for Grant SFRH/BD/73228/2010. This study was financially supported by FCT through the Project PEst-OE/QUI/UI0100/2011.

REFERENCES

(1) Grate, J. Acoustic Wave Microsensor Arrays for Vapor Sensing. *Chem. Rev.* **2000**, *100*, 2627−2648.

(2) Ricco, A.; Crooks, R.; Osbourn, G. Surface Acoustic Wave Chemical Sensor Arrays: New Chemically Sensitive Interfaces Combined with Novel Cluster Analysis To Detect Volatile Organic Compounds and Mixtures. *Acc. Chem. Res.* **1998**, *31*, 289−296.

(3) Mirmohseni, A.; Hassanzadeh, V. Application of Polymer-Coated Quartz Crystal Microbalance (QCM) as a Sensor for BTEX Compounds Vapors. *J. Appl. Polym. Sci.* **2001**, *79*, 1062−1066.

(4) Vogt, B.; Soles, C.; Lee, H.; Lin, E.; Wu, W. Moisture Absorption and Absorption Kinetics in Polyelectrolyte Films: Influence of Film Thickness. *Langmuir* **2004**, *20*, 1453−1458.

(5) Liang, C.; Yuan, C.; Warmack, R.; Barnes, C.; Dai, S. Ionic Liquids: A New Class of Sensing Materials for Detection of Organic Vapors Based on the Use of a Quartz Crystal Microbalance. *Anal. Chem.* **2002**, *74*, 2172−2176.

(6) Goubaidoulline, I.; Vidrich, G.; Johannsmann, D. Organic Vapor Sensing with Ionic Liquids Entrapped in Alumina Nanopores on Quartz Crystal Resonators. *Anal. Chem.* **2005**, *77*, 615−619.

(7) Shen, D.; Li, X.; Kang, Q.; Zhang, H.; Qi, Y. Monitor Adsorption of Acetone Vapor to a Room Temperature Ionic Liquid 1-Octyl-3-methylimidazolium Bromide by a Langasite Crystal Resonator. *Anal. Chim. Acta* **2006**, *566*, 19−28.

(8) Xua, X.; Canga, C.; Li, C.; Zhaoa, Z.; Li, H. Quartz Crystal Microbalance Sensor Array for the Detection of Volatile Organic Compounds. *Talanta* **2009**, *78*, 711−716.

(9) Rehman, A.; Hamilton, A.; Chung, A.; Baker, G.; Wang, Z.; Zeng, X. Differential Solute Gas Response in Ionic-Liquid-Based QCM Arrays: Elucidating Design Factors Responsible for Discriminative Explosive Gas Sensing. *Anal. Chem.* **2011**, *83*, 7823−7833.

(10) Xua, X.; Li, C.; Pei, K.; Zhaoa, K.; Zhaoa, Z.; Li, H. Ionic Liquids Used as QCM Coating Materials for the Detection of Alcohols. *Sens. Actuators, B* **2008**, *134*, 258−265.

(11) Ranke, J.; Stock, F.; Müller, A.; Stolte, S.; Störmann, R.; Bottin-Weber, U.; Jastorff, B. Lipophilicity Parameters for Ionic Liquid Cations and Their Correlation to in Vitro Cytotoxicity. *Ecotoxicol. Environ. Saf.* **2007**, *67*, 430−438.

(12) Huddleston, J. G.; Visser, A. E.; Reichert, W. M.; Willauer, H. D.; Broker, G. A.; Rogers, R. D. Characterization and Comparison of Hydrophilic and Hydrophobic Room Temperature Ionic Liquids Incorporating the Imidazolium Cation. *Green Chem.* **2001**, *3*, 156−164.

(13) Guan, W.; Ma, X.; Li, L.; Tong, J.; Fang, D.; Yang, J. Ionic Parachor and its Application in Acetic Acid Ionic Liquid Homologue 1-Alkyl-3-methylimidazolium Acetate {[$C_n$mim][OAc] (n = 2,3,4,5,6)}. *J. Phys. Chem. B* **2011**, *115*, 12915−12920.

(14) Branco, L.; Rosa, J.; Moura Ramos, J.; Afonso, C. Preparation and Characterization of New Room Temperature Ionic Liquids. *Chem.—Eur. J.* **2002**, *8*, 3671−3677.

(15) Vila, J.; Ginés, P.; Pico, J.; Franjo, C.; Jiménez, E.; Varela, L.; Cabeza, O. Temperature Dependence of the Electrical Conductivity in EMIM-Based Ionic Liquids: Evidence of Vogel−Tamman−Fulcher Behavior. *Fluid Phase Equilib.* **2006**, *242*, 141−146.

(16) Stolte, S.; Arning, J.; Bottin-Weber, U.; Pitner, W.; Welz-Biermann, U.; Jastorff, B.; Ranke, J. Effects of Different Head Groups and Modified Side Chains on the Cytotoxicity of Ionic Liquids. *Green Chem.* **2007**, *9*, 760−767.

(17) Restolho, J.; Mata, J.; Saramago, B. On the Interfacial Behavior of Ionic Liquids: Surface Tensions and Contact Angles. *J. Colloid Interface Sci.* **2009**, *340*, 82−86.

(18) Tariq, M.; Carvalho, P.; Coutinho, J.; Marrucho, I.; Lopes, J.; Rebelo, L. Viscosity of (C2−C14) 1-Alkyl-3-methylimidazolium Bis (Trifluoromethylsulfonyl) Amide Ionic Liquids in an Extended Temperature Range. *Fluid Phase Equilib.* **2011**, *301*, 22−32.

(19) Batchelor, T.; Cunder, J.; Fadeev, A. Wetting Study of Imidazolium Ionic Liquids. *J. Colloid Interface Sci.* **2009**, *330*, 415−420.
(20) Köhler, R.; Restolho, J.; Krastev, R.; Shimizu, K.; Lopes, J.; Saramago, B. Liquid- or Solid-like Behavior of [omim][BF_4] at a Solid Interface? *J. Phys. Chem. Lett.* **2011**, *2*, 1551−1555.
(21) Restolho, J.; Serro, A.; Mata, J.; Saramago, B. Viscosity and Surface Tension of 1-Ethanol-3-methylimidazolium Tetrafluoroborate and 1-Methyl-3-octylimidazolium Tetrafluoroborate over a Wide Temperature Range. *J. Chem. Eng. Data* **2009**, *54*, 950−955.
(22) Fendt, S.; Padmanabhan, S.; Blanch, H.; Prausnitz, J. Viscosities of Acetate or Chloride-Based Ionic Liquids and Some of Their Mixtures with Water or Other Common Solvents. *J. Chem. Eng. Data* **2011**, *56*, 31−34.
(23) Fowkes, F. Attractive Forces at Interfaces. *Ind. Eng. Chem.* **1964**, *56*, 40−52.
(24) Correia, N.; Ramos, J.; Saramago, B.; Calado, J. Estimation of the Surface Tension of a Solid: Application to a Liquid Crystalline Polymer. *J. Colloid Interface Sci.* **1997**, *189*, 361−369.
(25) Liu, F.; Shen, W. Forced Wetting and Dewetting of Liquids on Solid Surfaces and their Roles in Offset Printing. *Colloids Surf., A* **2008**, *316*, 62−69.
(26) Sauerbrey, G. Verwendung von Schwingquarzen zur Wägung dünner Schichten und Microwägung. *Z. Phys.* **1959**, *155*, 206−222.
(27) Lukkari, J.; Salomäki, M.; Ääritalo, T.; Loikas, K.; Laiho, T.; Kankare, J. Preparation of Multilayers Containing Conjugated Thiophene-Based Polyelectrolytes. Layer-by-Layer Assembly and Viscoelastic Properties. *Langmuir* **2002**, *18*, 8496−8502.
(28) Kanazawa, K.; Gordon, J., II. The Oscillation Frequency of a Quartz Resonator in Contact with a Liquid. *Anal. Chim. Acta* **1985**, *175*, 99−105.
(29) Martin, S.; Granstaff, V.; Frye, G. Characterization of a Quartz Crystal Microbalance with Simultaneous Mass and Liquid Loading. *Anal. Chem.* **1991**, *63*, 2272−2281.
(30) Francesco, F.; Calisi, N.; Creatini, M.; Melai, B.; Salvoc, P.; Chiappe, C. Water Sorption by Anhydrous Ionic Liquids. *Green Chem.* **2011**, *13*, 1712−1717.
(31) Cuadrado-Prado, S.; Dominguez-Pérez, M.; Rilo, E.; Gracia-Garabal, S.; Segade, L.; Franjo, C.; Cabeza, O. Experimental Measurement of the Hygroscopic Grade on Eight Imidazolium Based Ionic Liquids. *Fluid Phase Equilib.* **2009**, *278*, 36−40.
(32) Shi, W.; Damodaran, K.; Nulwalae, H. B.; Luebke, D. R. Theoretical and Experimental Studies of Water Interaction in Acetate Based Ionic Liquids. *Phys. Chem. Chem. Phys.* **2012**, *14*, 15897−15908.
(33) Restolho, J.; Mata, J. L.; Shimizu, K.; Canongia Lopes, J. N.; Saramago, B. Wetting Films of Two Ionic Liquids: [C_8mim][BF_4] and [C_2OHmim][BF_4]. *J. Phys. Chem. C* **2011**, *115*, 16116−16123.
(34) Sun, Y. Sorption/Desorption Properties of Water Vapor in Poly(2-thydroxyethyl methacrylate): 2. Two-Stage Sorption Models. *Polymer* **1996**, *37*, 3921−3928.
(35) Schwarz, B.; Schönhoff, M. Surface Potential Driven Swelling of Polyelectrolyte Multilayers. *Langmuir* **2002**, *18*, 2964−2966.